Nitrogen isotope and trace metal analyses from the Mingolsheim core (Germany): Evidence for redox variations across the Triassic-Jurassic boundary

Tracy M. Quan,[1] Bas van de Schootbrugge,[3] M. Paul Field,[1] Yair Rosenthal,[1] and Paul G. Falkowski[1,2]

Received 21 March 2007; revised 11 December 2007; accepted 18 January 2008; published 10 May 2008.

[1] The Triassic-Jurassic (T-J) boundary was one of the largest but least understood mass extinction events in the Phanerozoic. We measured bulk organic nitrogen and carbon isotopes and trace metal concentrations from a core near Mingolsheim (Germany) to infer paleoenvironmental conditions associated with this event. Poorly fossiliferous claystones across the boundary have relatively low $\delta^{15}N$ values and low concentrations of redox-sensitive elements, characteristic of an oxic environment with significant terrestrial input. The Early Jurassic features enrichment in $\delta^{15}N$ coincident with high redox-sensitive element concentrations, indicating an increase in water column denitrification and decreased oxygen concentrations. These redox state variations are concordant with shifts in abundance and species composition in terrestrial and marine microflora. We propose that the mass extinction at the T-J boundary was caused by a series of events resulting in a long period of stratification, deep-water hypoxia, and denitrification in this region of the Tethys Ocean basin.

Citation: Quan, T. M., B. van de Schootbrugge, M. P. Field, Y. Rosenthal, and P. G. Falkowski (2008), Nitrogen isotope and trace metal analyses from the Mingolsheim core (Germany): Evidence for redox variations across the Triassic-Jurassic boundary, *Global Biogeochem. Cycles*, *22*, GB2014, doi:10.1029/2007GB002981.

1. Introduction

[2] A variety of scenarios have been proposed to explain the mass extinction event at the Triassic-Jurassic (T-J) boundary (ca. 200 Ma) including asteroid impacts [*Olsen et al.*, 2002], magmatic outgassing and volcanism [*Hesselbo et al.*, 2002; *Knight et al.*, 2004; *Marzoli et al.*, 2004; *Pálfy*, 2003], global warming [*McElwain et al.*, 1999; *Tanner et al.*, 2004] and sea level change [*Hallam and Wignall*, 1999]. While the general consensus seems to indicate gradual extinction [e.g., *Hallam*, 2002; *Kiessling et al.*, 2007; *Tanner et al.*, 2004; *Vaughan and Storey*, 2007], other interpretations seem to favor a more abrupt event [*Whiteside et al.*, 2007]; the duration of the environmental instability and recovery is not well constrained. Complicating the interpretation are the presence of unconformities within sections, the lack of a distinct, well-defined boundary, and the difficulty of correlating marine and terrestrial records. Summaries of the various hypothesis for triggering the mass extinction as well as the difficulties of interpreting the T-J boundary in general can be found in *Hesselbo et al.* [2007] and *Tanner et al.* [2004].

[3] Here, we investigate a unique succession of shallow marine sediments spanning the T-J boundary (upper Rhaetian to lower Sinemurian) that provides information related to the cause and duration of the environmental changes during and following the mass extinction event.

[4] In order to better understand the processes that occurred during the mass extinction and their relationship to any of the proposed causes, many investigators have measured $\delta^{13}C$ of both organic and inorganic carbon fractions in a variety of stratigraphic sections spanning the T-J boundary. A negative carbon isotope excursion in both carbonate and organic carbon profiles around the stratigraphically defined boundary has been described from several locations, including Austria [*Kuerschner et al.*, 2007; *McRoberts et al.*, 1997], Hungary [*Pálfy et al.*, 2001, 2007], Canada [*Sephton et al.*, 2002; *Ward et al.*, 2001, 2004], Spain [*Gomez et al.*, 2007], and Italy [*Galli et al.*, 2005, 2007]. Organic carbon profiles from England [*Hesselbo et al.*, 2002], Canada [*Williford et al.*, 2007], and Nevada [*Guex et al.*, 2004] have two such negative excursions: a relatively rapid excursion close to the T-J boundary, and a more prolonged phase of low C isotope values occurring during the early Jurassic. Palynological analysis relates these negative $\delta^{13}C$ excursions to the mass extinction at the T-J boundary [*Galli et al.*, 2005; *Guex et al.*, 2004; *McRoberts et al.*, 1997; *Ward et al.*, 2004]. Here we examine changes in the nitrogen isotopes in organic matter preserved in samples

[1]Institute of Marine and Coastal Sciences, Rutgers University, New Brunswick, New Jersey, USA.
[2]Department of Earth and Planetary Sciences, Rutgers University, New Brunswick, New Jersey, USA.
[3]Institute of Geosciences, Johann Wolfgang Goethe University Frankfurt, Frankfurt, Germany.

0886-6236/08/2007GB002981$12.00

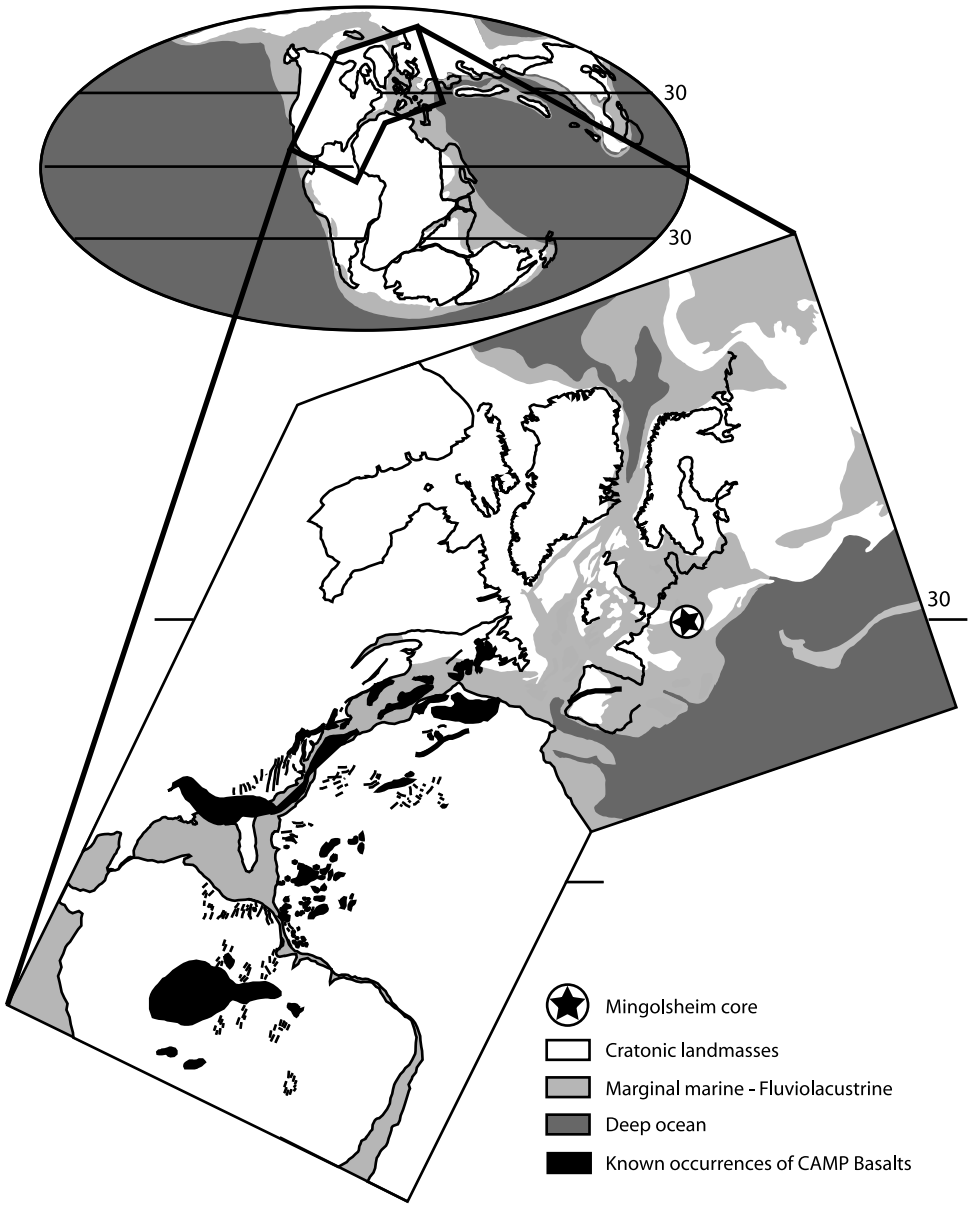

Figure 1. Paleogeographic reconstruction for the Late Triassic showing the location of the Mingolsheim core and the extent of the Central Atlantic Magmatic Province (CAMP estimates modified from *McHone* [2002]).

spanning the T-J boundary in an effort to understand how the cycle of this element changed in response to the extinction event, and the effect the change may have had on oceanic life.

[5] The $\delta^{15}N$ of the nitrate in the ocean is predominantly controlled by microbiological processes [*Wada*, 1980] that are coupled to the oxygen and carbon cycles [*Fennel et al.*, 2005]. In the modern ocean, variations in the nitrogen isotopic signature of nitrate are strongly regulated by water column oxygen concentrations. A well-preserved organic sedimentary nitrogen isotope record at any location reflects two dominating end-member local processes superimposed on the average ocean $\delta^{15}N$ signal: nitrogen fixation, which results in a small, negative nitrate $\delta^{15}N$, and water column denitrification, which greatly enriches the $\delta^{15}N$ values of the residual nitrate. At low oxygen concentrations, denitrification is favored, resulting in the deposition of organic matter with enriched $\delta^{15}N$ values. High oxygen concentrations inhibit denitrification, resulting in the generation of isotopically lighter sedimentary organic matter. Since the environmental conditions under which the different nitrate uptake processes occur are known, the measured nitrogen isotopic ratio can be used potentially as a qualitative paleoproxy of redox state in the water column at a particular location. Bulk organic nitrogen isotope values have been used to determine the predominant water column nitrogen

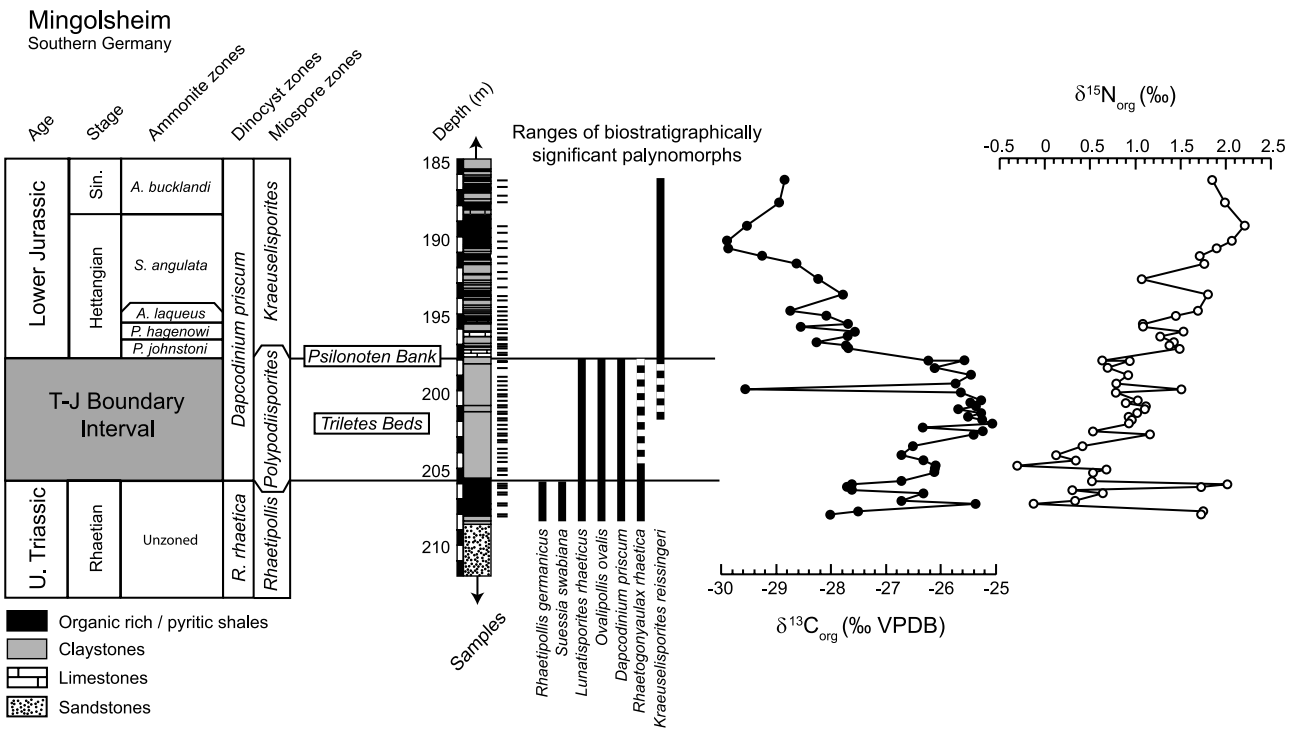

Figure 2. The stratigraphy and $\delta^{13}C_{org}$ and $\delta^{15}N_{org}$ profiles for the Mingolsheim core. Both profiles show distinctly different patterns in the Upper Triassic shales (208.63–205.6 m), the Triletes Beds (202.95–198.2 m) and the Hettangian-Sinemurian interval (198.2–186.25 m).

reaction in paleogeological as well as modern-day settings [e.g., *Altabet and Francois*, 1994; *Calvert et al.*, 2001; *Ganeshram et al.*, 1995, 2000, 2002]. Hence we propose that sedimentary $\delta^{15}N_{org}$ values reflect changes in the influence of water column redox conditions on the nitrogen cycle in the ocean through time.

[6] An independent, complimentary set of geochemical proxies of paleo-oxygen conditions are elemental redox proxies such as Fe, Mn, V, U, Mo, and Cd [*Algeo and Lyons*, 2006; *Brumsack*, 2006; *Elbaz-Poulichet et al.*, 2005; *Morford and Emerson*, 1999; *Raiswell et al.*, 2001]. Although variations in the enrichment or depletion of these metals in the sedimentary record reflect the concentration of oxygen in the sediments and the presence of S- species [*Elbaz-Poulichet et al.*, 2005; *Morford and Emerson*, 1999; *Tribovillard et al.*, 2006], redox conditions in the water column can also change the relative trace metal concentrations preserved in the underlying sediments [*Algeo and Lyons*, 2006; *Arnold et al.*, 2004; *Elbaz-Poulichet et al.*, 2005; *Raiswell et al.*, 2001; *Tribovillard et al.*, 2006]. While analyses of individual trace metals may give biased or misleading results due to factors such as organic matter complexation, micronutrient utilization, remobilization, or detrital input, the measurements of a broad suite of redox-sensitive trace metals can potentially serve as paleoredox proxies for water column conditions [*Tribovillard et al.*, 2006].

[7] In this paper we analyze $\delta^{15}N_{org}$, $\delta^{13}C_{org}$, and elemental profiles in a core from Mingolsheim, Germany, which crosses the T-J boundary. Nitrogen isotopes were measured in order to look at the changes that occur in the nitrogen cycle, and to determine the wider paleoenvironmental implications of redox conditions through this interval. Trace metal and rare earth elements were measured to independently infer both the redox state of the water column at the time of deposition and detrital input from the continents to the continental shelf through the Early Jurassic. We use these measurements in combination with mineralogical and palynological analyses to develop a plausible scenario for the T-J extinction in a region bordering the Tethys Ocean.

[8] The Mingolsheim core was drilled in 1968 near the town of Bad Mingolsheim in Southern Germany [*Hettich*, 1974]. The core is of great interest because it contains a more expanded Upper Triassic to Lower Jurassic succession than other outcrops and cores from southern Germany. Mingolsheim was situated in the depocenter of a local shallow marine basin (the Langenbrückener Trough; Figure 1). Drilling reached a total depth of 227 m covering the uppermost Triassic Keuper marls up to the Lower Jurassic Toarcian black shales. The investigated interval comprises the uppermost Rhaetian to lowermost Sinemurian from 208 m to 186 m (Figure 2). On the basis of the fossilized remains of marine phytoplankton (dinoflagellate cysts, acritarchs, and prasinophytes), the uppermost Rhaetian to Sinemurian strata reflect exclusively marine sedimentation (B. van de Schootbrugge et al., Acid rain and the demise of terrestrial ecosystems at the Triassic-Jurassic boundary,

Table 1. Organic Carbon Isotope and Nitrogen Isotope Measurements for the Mingolsheim Core[a]

Depth	$\delta^{15}N$, ‰	$\delta^{13}C$, ‰	%TOC
208.2	1.8	−28.0	*
208	1.8	−27.5	*
207.5	−0.1	−25.5	*
207.3	0.4	−26.7	*
206.8	0.7	−26.3	*
206.6	0.3	−27.6	*
206.4	1.8	−27.7	*
206.2	2.1	−27.6	*
206	0.6	−26.7	*
205.45	0.6	−26.1	*
205.23	0.7	−26.1	*
205	−0.3	−26.1	*
204.65	0.4	−26.3	*
204.3	0.2	−26.7	*
203.72	0.5	−26.5	*
202.95	1.2	−25.4	0.37
202.75	0.5	−25.2	0.30
202.25	0.9	−25.1	0.38
202	1.0	−25.2	0.40
201.8	0.9	−25.5	0.41
201.54	1.0	−25.3	0.42
201.3	1.1	−25.7	0.43
201.1	1.1	−25.4	0.44
200.9	0.9	−25.4	0.39
200.7	1.0	−25.3	0.42
200.18	0.8	−25.6	0.44
200	1.5	−29.6	0.44
199.6	0.8	−25.7	0.45
199.05	0.9	−25.5	0.43
198.56	0.7	−26.1	0.54
198.1	0.6	−26.2	0.41
198.1	0.9	−25.6	0.36
197.3	1.5	−27.7	0.37
197.1	1.4	−27.7	0.30
196.9	1.4	−28.3	0.70
196.5	1.3	−27.7	0.23
196.2	1.5	−27.6	0.34
195.9	1.1	−28.6	0.99
195.7	1.1	−27.7	0.83
195.14	1.5	−28.1	0.29
194.85	1.7	−28.7	1.61
193.75	1.8	−27.8	1.07
192.75	1.1	−28.2	0.58
191.75	1.8	−28.6	2.09
191.25	1.7	−29.3	2.23
190.75	1.9	−29.9	2.58
190.25	2.1	−29.9	3.13
189.25	2.2	−29.5	5.58
187.75	2.0	−28.9	1.39
186.25	1.9	−28.8	4.01

Samples marked with an * were not measured.

[a]Selected samples were also analyzed for % total organic carbon (%TOC).

submitted to *Nature Geosci.*, 2008, hereinafter referred to as B. van de Schootbrugge et al., submitted manuscript, 2008), even though sea level fluctuations likely led to significant changes in bathymetry. The T-J boundary is thought to lie within or at the base of the so-called "*Triletes Beds*" (205.6–198.2 m), a peculiar unit of carbonate poor claystones that are devoid in any macrofossil remains, but are extremely rich in trilete fern spores (B. van de Schootbrugge et al., submitted manuscript, 2008). Several characteristic Rhaetian pollen and dinoflagellate cysts, such as *Rhaetipollis germanicus* and *Suessia swabiana*, respectively, disappear at its base (Figure 2). Other typical Triassic pollen taxa, such as *Lunatisporites rhaeticus* and *Ovalipollis spp.*, disappear at its top. The duration of the Triletes Beds is difficult to constrain. On the basis of palynological evidence (e.g., last occurrence of *Rhaetipollis germanicus*), the Triletes Beds seem to correspond to the Zu-4 Member in Italy – an azoic, finely laminated limestone unit that has a variable thickness of up to 30 m and contains the T-J boundary at its base [*Galli et al.*, 2005, 2007].

[9] The Lower Jurassic at Mingolsheim is better constrained than the Upper Triassic based on ammonites [*von Hildebrandt and Schweizer*, 1992]. Starting with the so-called Psilonoten Bank and continuing with typical Lower Jurassic alternations of limestones, marls and organic rich shales, these beds comprise the Lower Hettangian *Caloceras johnstoni* Subzone (of the *Psiloceras planorbis* Zone), lowermost Middle Hettangian (*Alsatites liassicus* Zone), Upper Hettangian (*Schlotheimia angulata* Zone) and lowermost Sinemurian (*Arietites bucklandi* Zone). Although there is no evidence for a major erosional unconformity, the Jurassic ammonite fauna lacks representatives typical of the lowermost Jurassic *Psiloceras planorbis* Subzone. Therefore we cannot exclude a paraconformity between the top of the Triletes Beds and the base of the Psilonoten Bank (Figure 2). However, conditions may have been too shallow during deposition of the Triletes Beds to allow psiloceratid ammonites to migrate from the open Tethys into the Germanic Basin. Another explanation could be that the Psilonoten Limestone is highly condensed, marking the onset of a major flooding event [*Bloos*, 1976, 1999].

2. Methods

2.1. Sample Collection and Preparation

[10] Samples, collected at approximately 0.5 m intervals, were treated with 38% HCl prior to carbon and nitrogen isotopic analysis to remove all carbonate. The residues were rinsed several times with distilled water, dried for 3 d at 80° C and subsequently ground to a homogeneous powder using an agate mortar. For metal and TOC analysis, selected whole rock samples were powdered and homogenized by hand using a ceramic mortar and pestle and dried overnight at 60°C. Samples for TOC analysis were decarbonated in silver boats using 25% HCl, then measured with a Carlo Erba NA 1500 N/C/S analyzer using acetanilide as a standard. Replicate analyses had standard deviations of <0.01%.

[11] Whole rock digestions were performed by heating 60 mg of powdered sample with a 2:1 (v/v) mixture of HF:HNO_3 (Seastar Chemicals, Inc; Baseline grade) in Teflon vials for several days. The solutions were then evaporated, fluoride salts reduced by heating with concentrated HNO_3, then taken to near dryness again. Finally, the samples were fumed with perchloric acid (Fisher Scientific; trace metal grade), redissolved in 150 μl concentrated HNO_3 and sonicated for 30 min prior to final dilution with 450 μl of 1N HNO_3. Teflon beakers were cleaned by

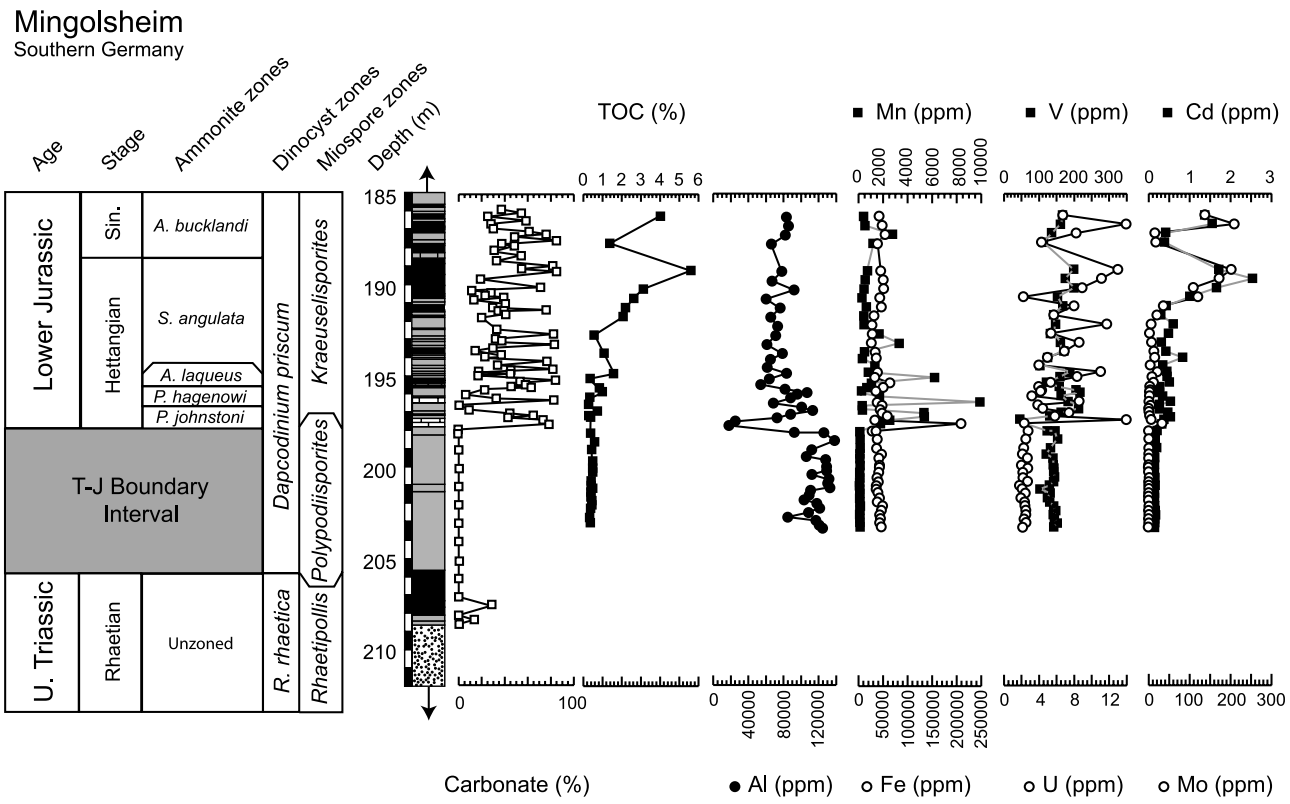

Figure 3. Elemental concentrations for Al, Fe, Mn, U, V, Mo, and Cd. All metal profiles were corrected for $CaCO_3$ content. Percent total organic carbon (TOC) and carbonate are also shown; carbonate measurements taken from *Hettich* [1974].

sequential boiling in 50% HCl and 50% HNO_3 (Fisher Scientific; trace metal grade).

2.2. Organic Carbon and Nitrogen Isotopes

[12] Carbon isotope analysis of TOC was subsequently performed using a Flash Elemental Analyzer 1112 (Thermoquest), connected to the continuous flow inlet system of a MAT 253 gas source mass spectrometer (Thermoquest) at the Institute of Geosciences (Goethe University Frankfurt). Depending on their TOC content sample aliquots of 3–10 mg were weighed and wrapped into tin capsules. At least two aliquots were prepared per sample. USGS 24 standard was analyzed along with the samples in order to prove for accuracy and precision. Both samples and standards reproduced within ±0.2‰.

[13] Nitrogen isotopes were measured using elemental analysis-isotope ratio mass spectrometry. Aliquots of powdered sample (25–35 mg) were sealed in silver capsules along with a vanadium oxide catalyst and combusted using a Eurovector elemental analyzer attached to a GV Instruments IsoPrime continuous flow isotope ratio mass spectrometer. NIST standards N1 (ammonium sulfate) and N3 (potassium nitrate), along with an in-house standard mix, were run between every 10 to 15 samples to calibrate the reference gas. Triplicate analyses of the Mingolsheim samples had a standard deviation of less than ±0.1‰. Variation in the in-house standard mix was determined to be ±0.2‰ (n = 42).

2.3. Metal Analyses

[14] Major (Al, Ca, Fe, and Mn) and trace elements (Cd, Mo, U, and V) were measured by an Inductively Coupled Plasma Optical Emission Spectrometer (ICP-OES, Vista Pro, Varian Inc., Australia) and a High Resolution Inductively Coupled Plasma Mass Spectrometer (HR-ICP-MS, Element-1, ThermoFinnigan, Bremen, Germany), respectively. Small volumes (<3 mL) were introduced to the ICP-OES using an SC-FAST system connected to a PFA μFlow nebulizer in an Apex-E desolvating unit (Elemental Scientific, Inc, Omaha, NE). This configuration provided 10× increase in sensitivity, 1000 fold wash out, three 10 s replicates and <0.5% signal stability in 48 s per sample. The HR-ICP-MS used a PFA μFlow nebulizer (Elemental Scientific, Inc, Omaha, NE) and a glass spray chamber for trace metal (Cd, Mo, U, and V) determination at resolutions appropriate to eliminate polyatomic interferences. Final concentrations calculated after normalization to internal standards, pseudo-standard addition and procedural blank subtraction (as described by *Cullen et al.* [2001]) exhibit better than +5% precision and accuracy. Detection limits for the ICP-OES were 50 ppm for Al, 40 ppm for Ca, 20 ppm for Fe, and 0.2 ppm for Mn;

Table 2. Elemental Concentrations for Al, Fe, Mn, U, V, Mo, and Cd in Whole Rock Samples[a]

Depth	Al (ppt)	Fe (ppt)	Mn (ppt)	Mo (ppm)	Cd (ppm)	U (ppm)	V (ppm)
203.4	124	46	0.14	0.33	0.14	2.09	142.0
203.18	121	43	0.12	0.30	0.15	2.49	150.8
202.95	117	44	0.12	0.33	0.14	2.30	143.8
202.75	85	43	0.12	0.52	0.17	2.51	142.3
202.5	108	47	0.14	0.48	0.17	2.49	146.0
202.25	120	49	0.15	0.30	0.15	2.41	140.8
202	118	39	0.13	0.27	0.14	2.38	130.7
201.8	104	42	0.13	0.31	0.14	1.95	123.5
201.54	109	40	0.13	0.37	0.15	2.45	131.2
201.3	110	36	0.12	0.27	0.11	2.07	101.8
201.1	133	36	0.12	0.49	0.15	1.80	130.8
200.9	131	41	0.12	0.34	0.13	2.65	140.9
200.7	132	38	0.12	0.61	0.15	2.19	143.9
200.4	112	41	0.13	0.30	0.14	2.14	142.5
200.18	129	41	0.13	0.30	0.14	2.67	142.9
200	129	43	0.13	0.43	0.15	2.00	141.2
199.6	128	42	0.13	0.37	0.14	2.66	140.5
199.4	106	47	0.13	0.29	0.13	2.08	121.0
199.05	112	37	0.15	0.29	0.19	2.26	132.6
198.56	138	38	0.14	0.37	0.16	2.51	151.5
198.1	126	36	0.16	0.66	0.20	2.73	144.3
198.1	92	28	0.14	0.41	0.20	2.75	124.0
197.7	177	210	1.79	27.65	0.32	2.33	55.8
197.5	248	33	2.51	6.76	0.37	13.91	45.0
197.3	72	59	5.40	2.23	0.52	5.76	130.4
197.1	88	49	5.29	1.10	0.47	7.41	162.7
196.9	113	45	3.40	1.10	0.26	4.45	211.2
196.7	101	48	3.14	4.80	0.26	3.84	218.0
196.5	68	38	9.86	1.14	0.52	8.56	183.0
196.2	89	39	1.75	1.46	0.34	3.14	164.1
196	96	38	0.20	1.20	0.29	4.10	214.4
195.9	106	35	0.26	2.31	0.24	4.27	206.1
195.7	81	50	0.70	2.46	0.28	3.97	156.7
195.45	54	63	1.05	11.90	0.50	5.28	121.5
195.14	64	34	6.17	7.20	0.45	8.33	159.3
194.85	83	38	0.80	21.24	0.44	11.03	188.3
194.5	62	37	1.39	3.20	0.34	3.96	107.3
194.09	65	36	0.36	15.31	0.83	4.95	128.0
193.75	79	34	0.51	12.61	0.42	6.90	163.3
193.25	61	26	3.30	6.96	0.31	8.55	161.0
192.75	71	28	1.67	1.58	0.48	5.37	142.0
192.25	73	27	0.45	6.08	0.60	11.71	146.1
191.75	65	31	0.41	19.29	0.30	5.68	137.2
191.25	76	46	0.64	35.08	0.42	7.98	167.0
190.75	60	43	0.29	120.10	1.01	2.20	152.8
190.25	92	51	0.46	108.88	1.66	8.88	200.2
189.75	67	50	0.55	171.59	2.54	11.12	174.1
189.25	78	54	0.70	200.63	1.71	13.01	198.4
187.75	66	39	1.22	17.60	0.38	4.27	112.3
187.25	82	54	2.76	15.03	0.41	8.27	136.1
186.75	86	48	0.52	209.03	1.55	13.94	161.9
186.25	83	41	0.43	140.22	1.35	6.68	170.5

[a]All concentrations in ppt (Al, Fe, Mn) or ppm (U, V, Mo, Cd). Concentrations for all elements corrected for $CaCO_3$ dilution effects by assuming all measured Ca was in carbonate form, then recalculating metal concentrations using the $CaCO_3$-free sample mass.

ICP-MS detection limits were 7 ppb for Mo, 0.7 ppb for Cd, 2 ppb for U, and 10 ppb for V.

3. Results

3.1. Nitrogen and Organic Carbon Isotopes

[15] Both nitrogen and organic carbon isotope values for the Mingolsheim core vary with depth and are coincident with shifts in lithology (Figure 2 and Table 1), ranging from $-0.3 \pm 0.1‰$ to $+2.2 \pm 0.1‰$ for nitrogen and $-29.9 \pm 0.1‰$ to $-25.1 \pm 0.1‰$ for C_{org}. In the Upper Rhaetian section of the core (208.63–205.6 m), prior to the T-J boundary, $\delta^{15}N_{org}$ values range widely from $-0.1 \pm 0.1‰$ to $+2.1 \pm 0.1‰$, with an average value of $+1.0 \pm 0.8‰$, while $\delta^{13}C_{org}$ values range from $-28.0 \pm 0.1‰$ to $-25.5 \pm 0.1‰$, with an average of $-27.1 \pm 0.8‰$. Values within the Triletes Beds (205.6–198.2 m) range from $+0.5 \pm 0.1‰$ to $+1.2 \pm 0.1‰$ and $-25.1 \pm 0.1‰$ to $-26.2 \pm 0.1‰$, for nitrogen and organic carbon isotopic values, respectively, with the exception of the single sample excursion at 200 m,

which had a $\delta^{15}N_{org}$ value of 1.5‰ and a $\delta^{13}C_{org}$ of -29.6 ± 0.1‰. For samples taken from the Hettangian-Sinemurian (198.2–186.25 m), the $\delta^{15}N_{org}$ values are isotopically heavier than those in the Triletes Beds, ranging from $+1.1 \pm 0.1$‰ to $+2.2 \pm 0.1$‰, with an average value of $+1.6 \pm 0.3$‰. Organic carbon isotope values from this interval ranged from -29.9 ± 0.1‰ to -27.6 ± 0.1‰ and were on average more depleted than the preceding Triletes Beds.

3.2. Metals

[16] Metal concentrations measured in representative, selected samples vary with depth and lithology in the core (Figure 3 and Table 2). The Triletes Beds are characterized by relatively high Al content, with an average concentration of 120 ± 10 ppt (1-SD). Average Fe and Mn concentrations within this interval are 41 ± 5 ppt and 0.13 ± 0.01 ppt, respectively. The variability in the concentrations of all three metals for this interval is <12%. The Triletes Beds also contain average concentrations of 2.3 ± 0.3 ppm, 140 ± 10 ppm, 0.4 ± 0.1 ppm, and 0.15 ± 0.02 ppm for U, V, Mo, and Cd, respectively. As with the major elements, the measured concentrations within this interval are very consistent, with variabilities <25%.

[17] Metal concentrations in the overlying Hettangian-Sinemurian are distinct from those in the underlying Triletes Beds (Figure 3 and Table 2). Compared to the Triletes Beds, the average concentrations for Al (70 ± 20 ppt) are lower in the Hettangian-Sinemurian, while the Fe (50 ± 30 ppt) and Mn (2 ± 2 ppt) concentrations are much higher and more variable. The range of concentrations for Al indicates an average decrease of more than 40 ppt and greater variability associated with lithology (> 27%). Comparative values for Fe and Mn are higher by 17 ppt and 9.7 ppt, respectively. Average concentrations for U, V, and Cd were, 7 ± 3 ppm, 160 ± 40 ppm, and 0.7 ± 0.6 ppm, respectively. These concentrations are enriched by 4.7 ppm, 19 ppm, and 0.55 ppm relative to the underlying Triletes Beds. Furthermore, the variability for these metals range from 26% to 86% of the average values. Mo concentrations are the most variable within this interval, ranging from a maximum of 209 ppm to a minimum of 1.1 ppm. The average Mo concentration for this interval is 40 ppm, approximately 39 ppm greater than the average Mo concentration in the Triletes Beds.

4. Discussion

4.1. Organic Nitrogen Isotopes

[18] Our measurements of nitrogen isotopes in the Mingolsheim core suggest there were distinct changes in the redox paleoenvironment across the T-J boundary in shallow marine regions bordering the Tethys Ocean (Figure 2). The organic nitrogen isotopic ratio in sediments has been shown to be a reliable record of the water nitrate isotopic ratio [*Altabet and Francois*, 1994]. The organic sedimentary nitrogen isotope record at any location reflects two dominating end-member processes: nitrogen fixation, characterized by a small, negative $\delta^{15}N$ signal and denitrification, which enriches $\delta^{15}N$ values. Remineralization of the light $\delta^{15}N$ organic matter resulting from N_2 fixation and nitrification with little denitrification results in a small, usually negative, fractionation of the nitrate pool, which is then translated to the sedimentary organic matter. In contrast, incomplete water column denitrification has a large, positive fractionation factor as the denitrification process strongly selects the lighter $^{14}NO_3^-$ molecules, leaving behind nitrate enriched in ^{15}N ($\delta^{15}N \sim +22$‰). The residual, isotopically heavy nitrate is reflected in the organic matter produced. As a result, the nitrogen isotope values for the surface nitrate pool, and thus bulk organic matter, reflect the relative strength of these two processes. Sedimentary $\delta^{15}N_{org}$ values in a predominantly nitrogen fixing or nitrifying system are characteristically lighter; $\delta^{15}N_{org}$ values for a system with higher levels of denitrification will be enriched.

[19] The sedimentary organic nitrogen isotope values can also indirectly reflect the redox state of the water column at the time of deposition. This can be explained conceptually by analyzing how the $\delta^{15}N$ signatures of organic matter would vary as oxygen concentrations increase in the surface waters (Figure 4). Nitrifying bacteria are obligate aerobes, while denitrifiers are facultative anaerobes. When there is no oxygen in the water column, nitrate cannot be formed and, as a result, the $\delta^{15}N$ is close to zero. As oxygen levels rise, so do the nitrate concentrations, leading to an increase in the levels of denitrification which, in turn, removes isotopically light nitrate. This trend of increasing nitrate concentrations and enriched $\delta^{15}N$ values via denitrification continues until water column oxygen reaches some critical threshold concentration where both denitrification and the $\delta^{15}N$ of the system are in kinetic equilibrium. If the oxygen increases beyond this "tipping point" (approximately 30 μM O_2), the amount of denitrification in the water column decreases as the higher oxygen level inhibits the denitrification reaction. With the decrease in the amount of denitri-

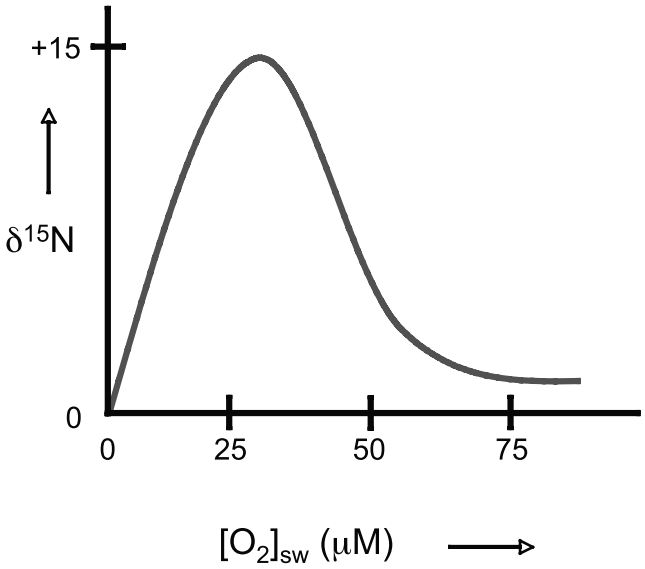

Figure 4. Conceptual model of changes in $\delta^{15}N$ values with changes in surface water oxygen levels. This graph shows that enriched $\delta^{15}N$ values are limited to a small range of water column O_2 concentrations that lie within the hypoxic/suboxic range.

fication, the $\delta^{15}N$ of the system also decreases, and returns again to lower values, reflecting the isotopic fractionation due to nitrification and nitrogen fixation. Using this model, we interpret enriched $\delta^{15}N$ values to be limited to a specific range of oxygen concentrations: enough oxygen must be present in the water column to allow for significant amounts of nitrate to be formed, but not so high as to inhibit denitrification. While it is clearly difficult to extrapolate this model to the geological record, based on contemporary N isotopic fractionations we estimate the range to be between 15 and 40 μM O_2, which lies within the hypoxic/suboxic levels of oxygen concentrations. Thus a significant positive shift in the $\delta^{15}N_{org}$ in a core implies the existence of a stratified or hypoxic water column concurrent with those estimated values.

[20] Below the Triletes Beds, i.e., prior to the T-J boundary, $\delta^{15}N_{org}$ profiles show very large and relatively rapid changes in nitrogen isotopic values through the Upper Rhaetian shales (Figure 2). Two peaks of highly enriched $\delta^{15}N_{org}$ appear in the record between 208.2 to 208.0 m and 206.4 to 206.2 m within the Upper Rhaetian. Both peaks show an enrichment of approximately 1.7‰ over the isotopic values for the surrounding samples, and seemingly reflect a period of environmental instability. In contrast, the $\delta^{15}N_{org}$ profile for the Triletes Beds is much less dynamic. Within the Triletes Beds, the $\delta^{15}N_{org}$ profile shows relatively depleted values (with the exception of the very sharp positive excursion around 200 m), then a shift to more enriched $\delta^{15}N_{org}$ values in the overlying Middle to Upper Hettangian (Figure 2). Inspection of the isotopic record in the context of factors influencing the nitrate pool outlined above suggests that denitrification was more pronounced in the water column when $\delta^{15}N_{org}$ values were higher. Since water column denitrification can only occur under reducing environments, the data imply that this shallow marine margin region of the Tethys Ocean became mostly hypoxic following the T-J boundary during the earliest Jurassic. Enriched $\delta^{15}N_{org}$ values also correlate with higher % total organic carbon (%TOC), which is as expected given the enhanced preservation of organic matter during anoxic periods (Figure 3 and Table 1). In contrast, the $\delta^{15}N_{org}$ values for samples from the Triletes Beds are more depleted, indicating less influence from denitrification on the nitrate pool, and thus higher levels of water column oxygen during this period.

4.2. Major and Redox-Sensitive Trace Metals

[21] We used Al concentrations to constrain detrital input. Terrestrial input to the core clearly dominates during the Triletes Beds with average Al concentrations of 120 ± 10 ppt (Table 2), only slightly higher than average Al concentrations for pelagic clays [*Taylor and McLennan*, 1985]. Fe and Mn are similar in concentration to average upper continental crust [*Taylor and McLennan*, 1985], further supporting the notion that the Triletes Beds are dominated by high detrital input.

[22] In contrast with the Triletes Beds, the lowermost Middle-Upper Hettangian and lowermost Sinemurian succession contains much lower Al levels and higher Fe, Mn, and carbonate concentrations (Figure 3 and Table 2). Al content decreased by 1.5 fold, while Fe increased by a factor of 1.2, and Mn increased by nearly 15 fold, indicating a distinct shift in major metal composition. The magnitude of the terrestrial input to the core as determined by Al concentrations is sharply reduced at the top of the Triletes Beds, and remains relatively low through the remainder of the Hettangian to Sinemurian.

[23] Trace metal concentrations in the Mingolsheim core show a similar relationship between concentration and lithology (Figure 3 and Table 2). All the redox-sensitive metals (U, Mo, Cd and V) have concentrations in the Triletes Beds similar to those of average upper continental crust and clays, and are present in enriched amounts in the Hettangian-Sinemurian interval relative to average marine shales and post-Archean Australian shale (PAAS) [*Taylor and McLennan*, 1985]. The concentrations measured in the Hettangian-Sinemurian interval of the core are more variable for all trace elements than in the Triletes Beds.

[24] To better understand the relationships between metal enrichment, lithology, and redox conditions, we removed the signal of the terrestrial input from the concentration measurements using Al content as a terrestrial indicator. We assume that metal concentrations within the clay (kaolinite, illite, and chlorite) dominated Triletes Beds represent the mean terrestrial input to the core. The average Triletes Bed concentration values were calculated for each metal and subtracted from the Hettangian-Sinemurian values after normalization to Al. The remaining concentration is interpreted as an enrichment and represents changes in redox conditions rather than shifts in terrestrial input or input via another lithologic phase. For example, average U concentrations in limestones has been measured to be less than 1 ppm [*Plank and Langmuir*, 1998]; the average Triletes Beds-adjusted concentrations for U in the Hettangian-Sinemurian interval are 5 ± 3 ppm. Similar enrichments in U, V, Mo, and Cd concentrations are seen in the Mingolsheim core (Figure 5).

[25] Increases in sedimentary Cd, Mo, V, and U have been shown to indicate low O_2 levels and the behavior of the individual metals is characteristic of specific depositional environments [*Morford and Emerson*, 1999; *Tribovillard et al.*, 2006]. Uranium and vanadium enrichment can occur in suboxic/anoxic environments that are sulfide-free, while enrichments of Cd and Mo require the presence of free H_2S species (i.e., euxinic conditions) [*Algeo and Maynard*, 2004]. Since individual metals often have complex redox chemistries, we have chosen to analyze all four redox-sensitive metals, Mo, Cd, U, and V, rather than any one particular element [*Tribovillard et al.*, 2006]. All four metals increase in concentration in the Sinemurian-Hettangian relative to the Triletes Beds, indicating that redox conditions in the water column and sediments changed from the oxic to suboxic/anoxic coincident with the shift in deposition from the Triletes Beds to the Hettangian-Sinemurian lithology. The adjusted U and V concentrations within the Hettangian-Sinemurian interval show a ten-fold excess over the average concentrations in the Triletes Beds (Figure 5). Since the adjusted metal concentrations for U and V remain relatively constant within the Hettangian-Sinemurian interval, we interpret these metal profiles as reflecting the change from oxic to suboxic conditions, but not differences between

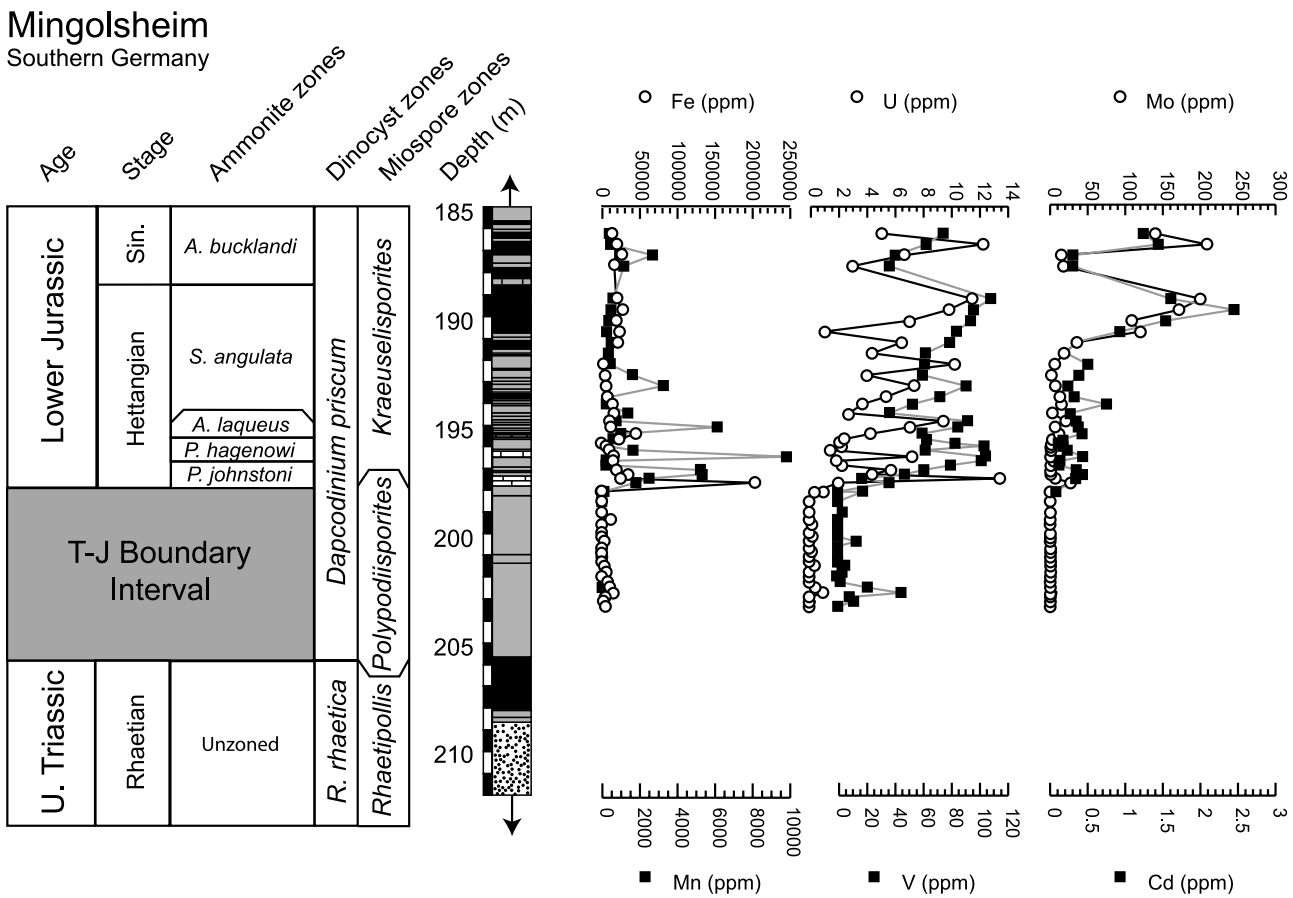

Figure 5. U, V, Mo, and Cd enrichment profiles for the Mingolsheim core. The average concentration for each metal within the Triletes Bed (202.95–198.2 m) was calculated and assumed to be detrital input. The authigenic metal concentrations were determined by subtracting the Al-normalized Triletes Bed concentrations from the measured concentrations.

suboxic and anoxic conditions. Both metals have similar profiles throughout the core, indicating that they reflect environmental shifts in the water column and sediments rather than changes in the input of the individual metals. Profiles for these metals also correlate well with the $\delta^{15}N_{org}$ measurements, as samples containing higher concentrations of U and V also tend to be enriched in $\delta^{15}N_{org}$ (Figure 6).

[26] Adjusted concentrations for Cd and Mo also reflect a distinct change to anoxic conditions across the T-J boundary through the Hettangian-Sinemurian (Figure 5). Concentrations of Cd and Mo are more sensitive to changes in sulfide concentrations [*Algeo and Maynard*, 2004; *Morford and Emerson*, 1999; *Tribovillard et al.*, 2006], so the lack of enrichment soon after the peak at 198.2 m indicates that the sulfide levels may have decreased, though it is likely that the bottom waters and sediments remained suboxic/anoxic. The second enrichment period between 191.25–187.75 m corresponds well with an extended period of organic rich shale deposition in the core, indicating another large sulfide enriched euxinic period, probably greater than the initial excursion at 198.2 m. Samples with high Cd and Mo concentrations also tend to have higher $\delta^{15}N_{org}$ values, indicating periods where the oxycline was higher in the water column, thus increasing the amount of suboxic waters available for denitrification (Figure 6). These results support our hypothesis that the Hettangian to lowermost Sinemurian interval represents a time of fluctuating hypoxic/anoxic to euxinic conditions in the bottom water and sediments, resulting in the enrichment of $\delta^{15}N_{org}$ values via denitrification and increased metal concentrations.

[27] The Triletes Beds-adjusted Fe and Mn also show periods of enrichment during the Hettangian-Sinemurian interval, but the profiles for these elements do not seem to simply reflect oxygen levels (Figure 5). While both Fe and Mn concentrations show a dramatic increase in concentration in the Psilonoten Bank, the patterns of enrichment for Mn and Fe do not correspond to that of the other metals during this anoxic interval. In particular, the lack of a distinct enrichment peak between 191.25–187.75 m seen in all the other redox-sensitive metals implies that Fe and Mn may also be influenced by other chemical or lithological effects. With this in mind, we consider Fe and Mn to be unreliable recorders of redox conditions in this core, per-

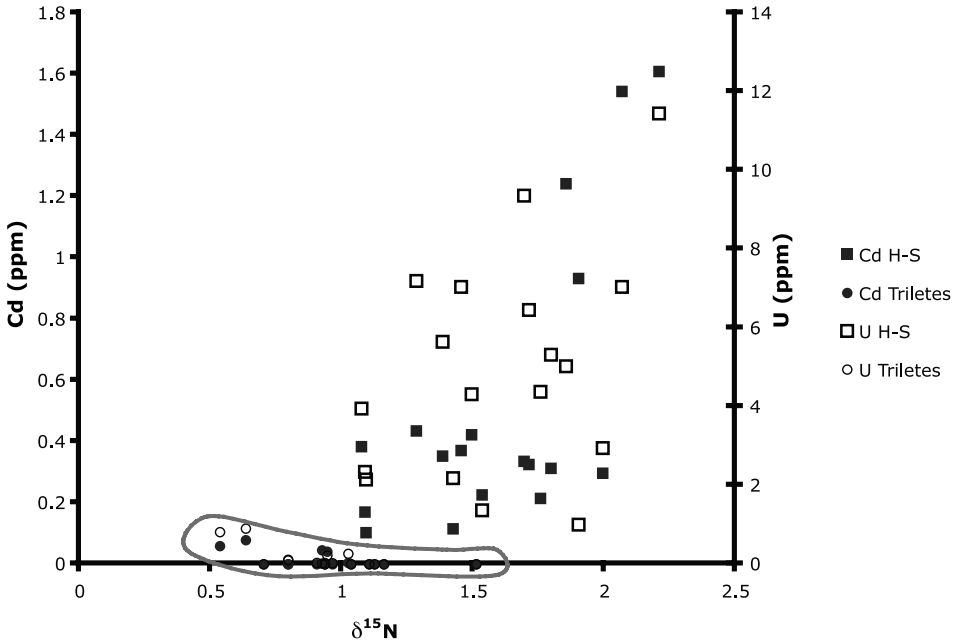

Figure 6. Authigenic U (filled symbols) and Cd (open symbols) concentrations plotted versus the measured $\delta^{15}N_{org}$ values for the Mingolsheim core. Samples can be separated into two distinct populations depending on their location in the core. Samples from the circled Triletes Bed (202.95–198.2 m; circle symbols) for both metals have a different correlation with $\delta^{15}N_{org}$ compared to samples from the Hettangian-Sinemurian (H-S) interval (198.2–186.25 m; square symbols). Correlations with $\delta^{15}N_{org}$ for V and Mo are similar to U and Cd respectively.

haps due to the potential for Mn remobilization and for detrital Fe input.

[28] The results from the redox-sensitive metal analysis of the Mingolsheim core can be separated into two pairs of metals: U and V, which seem to show enrichments when the oxygen level drops into suboxic or anoxic levels; and Mo and Cd, which generally reflect variations in sulfide concentrations, indicating euxinic conditions (Figure 5). Both pairs of metals indicate authigenic enrichment due to the onset of hypoxia/anoxia that occurs across the T-J boundary and into the middle Hettangian, and occasionally reappears throughout the upper Hettangian through the lowermost Sinemurian. In addition, the sharp variations in the enrichment profiles for U, V, Mo and Cd through the limestone/shale interval indicate that this environment was very dynamic, and that oxygen and sulfide levels probably fluctuated during the deposition of these sediments. It is most likely that the bottom water was hypoxic for the majority of the period, while the sediments were fully anoxic or even euxinic.

4.3. Correlation of Carbon and Nitrogen Isotopes

[29] Organic carbon isotopic values were measured on decarbonated samples and are shown in Figure 2 and Table 1. As with the nitrogen isotopes, there are three distinct intervals of the core: the large shifts seen in the Upper Rhaetian shales (208.63–205.6 m), the relatively enriched $\delta^{13}C$ section through the Triletes Beds and the more depleted values in the Hettangian-Sinemurian. This profile is also very similar to those from other T-J boundary records, including both the initial light isotope excursion (at 200 m) and the main isotope excursion (198.2–186.25 m) [e.g., *Guex et al.*, 2004; *Hesselbo et al.*, 2002; *Williford et al.*, 2007]. An inverse relationship between the $\delta^{13}C_{org}$ and $\delta^{15}N_{org}$ profiles can be seen throughout the core with only a few exceptions (Figure 2). Samples enriched in $^{15}N_{org}$ are also characterized by depleted $\delta^{13}C_{org}$ values, and vice versa. This inverse correlation is particularly noticeable for the major isotope excursions in the middle of the Triletes Beds and the longer excursion in the Hettangian-Sinemurian.

[30] The distinct inverse correlation between the nitrogen and carbon isotopes throughout the core seems to indicate that whatever process enriched one isotope depleted the other, and vice versa. This may not be the only possibility; carbon and nitrogen isotopes measured from the Toarcian (Early Jurassic) ocean anoxic event (OAE) also show an inverse relationship, but the authors conclude that the two events are independent of each other [*Jenkyns et al.*, 2001]. While we have not been able to conclusively identify the cause of the negative carbon isotope excursion, the fact that it is replicated in several spatially diverse sections seems to indicate that the isotopic signal is global.

[31] In the modern ocean, nitrogen isotopes reflect regional shifts in the nitrate pool, rather than a global signature. No other nitrogen isotope measurements have been published from this time period. Consequently, although it is premature to reach a strong conclusion about

whether the denitrification signal we see in the Early Jurassic is also found at other locations, it is very interesting that a recorder of "local" processes, such as $\delta^{15}N_{org}$, is correlated to a global signal, as illustrated by the various $\delta^{13}C$ records shown in this paper and others.

4.4. $\delta^{15}N_{org}$ and Metal Comparisons

[32] The combination of trace metal data and the nitrogen isotopes give some clues regarding the paleoenvironments of the Mingolsheim area from the Late Triassic through the T-J boundary into the Early Jurassic. The Upper Rhaetian shales are characterized by relatively quick shifts in environment from periods of enriched $\delta^{15}N_{org}$/depleted $\delta^{13}C_{org}$ to depleted $\delta^{15}N_{org}$/enriched $\delta^{13}C_{org}$ (Figure 2). The $\delta^{15}N_{org}$ profile seems to indicate that the relative intensity of denitrification, and thus bottom water oxygen levels, changed frequently during this time period. While metal concentrations were not measured in these samples, based on the data from the rest of the core we would expect confirmation of the redox changes in the late Triassic shales. In the Triletes Beds containing the T-J boundary, nitrogen isotope values are low, and redox-sensitive trace metal concentrations are relatively low, indicating that water column conditions were probably oxic during this time. High Al concentrations seem to indicate that terrestrial input was significant during the Triletes Beds as well (Figure 3). The Hettangian-Sinemurian interval is distinctly different than the Triletes Beds beneath it. The Hettangian-Sinemurian interval is characterized by enriched $\delta^{15}N_{org}$, and higher concentrations of redox-sensitive trace metals, indicating that denitrification was occurring in a low oxygen water column. The decrease in Al concentrations in this zone implies that terrestrial input to the area either decreased in strength or ceased altogether, reflecting the shift from clays to shales and limestones.

[33] The development of a hypoxic or anoxic marine environment during the Late Triassic to Early Jurassic interval has been hypothesized based on paleoenvironmental models [*van de Schootbrugge et al.*, 2007]. Anoxia caused by a decrease in oceanic circulation has been hypothesized to result from events such as increased CO_2 [*Huynh and Poulsen*, 2005] and global warming resulting from greenhouse gas input [*Kidder and Worsley*, 2004], two of the hypothetical root scenarios for the T-J mass extinction. Evidence for anoxia has been found in sections across the T-J boundary [*Hallam and Wignall*, 2000] and other minor Triassic extinction events [*Tanner et al.*, 2004], though it is unknown whether anoxia caused the mass extinction or resulted from other events [*Twitchett*, 2006].

4.5. Comparisons Between $\delta^{15}N_{org}$, Redox-Sensitive Elements and Primary Producers

[34] The palynology of the Mingolsheim core also provides a picture of the paleoconditions of the water column through the T-J boundary and into the Lower Jurassic. In brief, the distribution of both terrestrial and marine taxa shows a succession of drastic changes within this time period that runs parallel to changes observed in nitrogen isotopes and trace metal abundance. A dramatic change in terrestrial vegetation occurred at the T-J boundary from arborescent flora (conifers, seed ferns, cycads and ginkgophytes) to predominantly herbaceous flora (ferns and fern allies) within the Triletes Beds. This "fern spike" was succeeded during the Hettangian by an impoverished vegetation assemblage dominated by cheirolepid and taxodiaceous conifers and lycopods (B. van de Schootbrugge et al., submitted manuscript, 2008).

[35] Marine phytoplankton present during positive $\delta^{15}N_{org}$ excursions are often dominated by organisms that prefer stratified waters, and lower oxygen conditions. Preceding the T-J boundary, phytoplankton populations are dominated by typical Late Triassic cyst-producing dinoflagellates, which decrease in abundance during deposition of the Triletes Beds. During the Hettangian we observe first an increase in abundance of acritarchs followed by assemblages dominated by prasinophytes (B. van de Schootbrugge et al., submitted manuscript, 2008). Hence phytoplankton assemblages provide further evidence for an increase in stratification and development of anoxic bottom waters with the disappearance of cyst-producing dinoflagellates, that need oxygenated bottom waters, and the proliferation of chlorophytes (green algae) that have wholly planktonic life-cycles that play out in the water column and prefer reduced forms of nitrogen [*van de Schootbrugge et al.*, 2007].

4.6. A Plausible Scenario for the T-J Boundary

[36] If all the evidence from carbon and nitrogen isotopes, trace metals, and palynology is combined, a scenario for paleoenvironmental changes as recorded in the Mingolsheim core can be outlined. The events that occurred at the T-J boundary are increasingly linked with the pulsed eruption of flood basalts in Central Atlantic Magmatic Province (CAMP), releasing large quantities of SO_2 and CO_2 into the atmosphere over a time span of 500 Ka to 1.5 Ma [*Cohen and Coe*, 2002; *Hesselbo et al.*, 2002; *Knight et al.*, 2004; *Marzoli et al.*, 2004; *Pálfy*, 2003]. Though estimates of the geological extent of the CAMP suggest that the basalts themselves did not reach Mingolsheim (Figure 1), it is highly likely that the aerosols released by a "superplume" would be globally distributed [*Vaughan and Storey*, 2007]. Sulfur aerosols would initially cause brief disturbance on a regional scale in the form of acid rain, polluted soils, disruption of photosynthesis and cooling [*Robock*, 2000]. Long-term build-up of carbon dioxide would lead to global warming even after volcanic activity had ceased. These two contrasting effects are reflected in our data obtained from Mingolsheim.

[37] Before the T-J boundary, shallow seas were well populated with phytoplankton, mainly dinoflagellates with some acritarchs and prasinophytes present. The terrestrial vegetation on nearby landmasses was dominated by arborescent flora consisting mainly of conifers, cycads and ginkgophytes, suggestive of relatively warm and arid conditions. Nitrogen isotopes indicate that water column oxygen levels in this region of the Tethys Ocean were relatively unstable.

[38] The SO_2 produced by volcanism rained out of the atmosphere and acidified the soils, increasing the rate of weathering. A large amount of Al-containing clays (illite, chlorite, and kaolinite) were washed into the ocean, creating

the clay-rich Triletes Beds that marks the T-J boundary transition in the Mingolsheim core. Together with increased erosion from the land, we observe a rapid change in vegetation from a flora dominated by arborescent gymnosperms to an herbaceous flora consisting mainly of ferns and fern allies. We suggest that forest declined in response to soil acidification and that many of the pteridophytes were better adapted to living in these acidified environments [*Kuerschner et al.*, 2007; *Mills and Schindler*, 1986; *Stokes*, 1986]. This volcanic event(s) also led to a drastic decrease in phytoplankton abundance. Nitrogen isotopes and trace metals indicate that the water column at this time was oxic, though sea level was shallow [*Hallam*, 2001].

[39] The aerosol SO_2 was removed from the atmosphere on timescales of decades, though the CO_2 greenhouse remained for thousands of years. Weathering input was decreased resulting in the deposition of Al-poor shales and limestones during the Hettangian-Sinemurian. This decrease in weathering input under high pCO_2 conditions may indicate that the easily weathered soils had not fully recovered from the prior intense erosion. Nitrogen isotope values are enriched during this time, implying that denitrification occurred in a low oxygen zone within the water column. Redox-sensitive trace metal concentrations are generally high, confirming the presence of a predominantly hypoxic bottom water environment at this site, similar to the modern-day Black Sea. This stratification is probably due to a salinity gradient or a decreased oceanic circulation [*van de Schootbrugge et al.*, 2007]. Stratification may have also driven the shift from dinoflagellates to acritarchs to chlorophytes in the recovering phytoplankton population, as the latter two taxa are thought to be more adapted to stratified waters. The anoxic bottom waters also resulted in the deposition of carbon-rich lithology of interbedded limestones and black shales. The driving forces behind the negative excursions present in the $\delta^{13}C$ record are still debated; possible causes include recycling of isotopically light terrestrial carbon and/or input of isotopically light methane hydrates. These conditions fundamentally altered marine ecosystems, leading to the emergence of a diverse group of eukaryotic phytoplankton and differing food web structures in the Jurassic.

5. Conclusions

[40] Measurement of the nitrogen and organic carbon isotopes and trace metals in samples from the Mingolsheim core have provided details of the paleoenvironment in a marginal area of the Tethys Ocean across the T-J boundary. The presence of enriched values for the $\delta^{15}N_{org}$ of bulk organic nitrogen in sections of the core that also show relatively high concentrations of redox-sensitive trace metals such as U, V, Cd, and Mo indicates that nitrogen isotopes are an accurate proxy for the oxygen concentration levels in the water column. Enrichment of heavy nitrogen isotopes during the Early Jurassic implies increasing denitrification, and thus an increased zone of water column anoxia during this time period.

[41] It has yet to be determined whether the relationship between bulk organic matter $\delta^{15}N_{org}$ and trace metal concentration holds for all environmental situations. While nitrogen isotopes can indicate shifts to higher amounts of denitrification, and thus lower water column oxygen levels, it is unclear whether these lower oxygen levels will automatically translate to detectable enrichments in redox-sensitive trace metals, due to the complexities of trace metal deposition. As a result, more studies measuring both nitrogen isotopes and trace metals in a stratigraphic section are necessary to develop a rigorous correlation between $\delta^{15}N_{org}$ value and paleoredox levels.

[42] It is also unknown whether the reconstructed sequence of events at the T-J boundary of Mingolsheim is unique to this location or also seen on broader regional or global levels. Our carbon isotope data is very similar to the profiles measured from a variety of locations, indicating that this core records carbon cycle processes on a global level. Since nitrogen isotopes are generally considered to reflect regional rather than global processes, it cannot be assumed that the denitrification and hypoxic water column profiles will be found elsewhere in the world. Similarly, while volcanism has been previously identified as a potential cause for the mass extinction, our hypothetical scenario of acid weathering resulting in a large detrital input to the coastal areas, then leading to a stratified water column has yet to be confirmed in other sections. Additional measurements of both nitrogen isotopes and trace metals are necessary to better characterize the global nitrogen cycle and the oxygen levels at the T-J boundary and in the Early Jurassic.

[43] **Acknowledgments.** The authors thank Linda Godfrey for her help with the nitrogen isotope measurements, and Paul Field and the Rutgers Inorganic Analytical Laboratory for assistance with the OES and ICP-MS analyses. Volker Schweizer (University of Heidelberg, Germany) is thanked for providing access to the Mingolsheim core. This research was supported by the Agouron Foundation, the Jet Propulsion Laboratory, the Terrestrial Planet Finder team, NASA Exobiology program and Rutgers University. TMQ would also like to thank the IMCS Postdoctoral Fellowship program. BvdS acknowledges financial support from the Deutsche-Forschungsgemeinschaft Project Scho-1216/2-1.

References

Algeo, T. J., and T. W. Lyons (2006), Mo-total organic carbon covariation in modern anoxic marine environments: Implications for analysis of paleoredox and paleohydrographic conditions, *Paleoceanography*, *21*, PA1016, doi:10.1029/2004PA001112.

Algeo, T. J., and J. B. Maynard (2004), Trace-element behavior and redox facies in core shales of Upper Pennsylvanian Kansas-type cyclothems, *Chem. Geol.*, *206*, 289–318.

Altabet, M. A., and R. Francois (1994), Sedimentary nitrogen isotopic ratio as a recorder for surface ocean nitrate utilization, *Global Biogeochem. Cycles*, *8*(1), 103–116.

Arnold, G. L., A. D. Anbar, J. Barling, and T. W. Lyons (2004), Molybdenum isotope evidence for widespread anoxia in mid-Proterozoic oceans, *Science*, *304*, 87–90.

Bloos, G. (1976), Untersuchungen über Bau und Entstehung der Feinkörnigen Sandsteine des Schwarzen Jura alpha - Hettangium und tiefste Sinemurium) im schwäbischen Sedimentationsbereich, *Arbeiten des Instituts für Geologie und Paläontologie der Universität Stuggart N.F.*, *71*, 1–269.

Bloos, G. (1999), Aspekte der Wende Trias/Jura, in *Trias: Eine Ganz Andere Welt*, edited by N. Hauschke and V. Wilde, pp. 43–68, Verlag Dr. Friedrich Pfeil, Munich.

Brumsack, H.-J. (2006), The trace metal content of recent organic carbon-rich sediments: Implications for cretaceous black shale formation, *Palaeogeogr. Palaeoclimatol. Palaeoecol.*, *232*, 344–361.

Calvert, S. E., T. F. Pedersen, and R. E. Karlin (2001), Geochemical and isotopic evidence for post-glacial palaeoceanographic changes in Saanich Inlet, British Columbia, *Mar. Geol.*, *174*, 278–305.

Cohen, A. S., and A. L. Coe (2002), New geochemical evidence for the onset of volcanism in the Central Atlantic magmatic province and environmental change at the Triassic-Jurassic boundary, *Geology*, *30*(3), 267–270.

Cullen, J. T., M. P. Field, and R. M. Sherrell (2001), Determination of trace elements in filtered suspended marine particulate material by sector field HR-ICP-MS, *J. Anal. Atomic Spectrosc.*, *16*, 1307–1312.

Elbaz-Poulichet, F., et al. (2005), Sedimentary record of redox-sensitive elements (U, Mn, Mo) in a transitory anoxic basin (the Thau lagoon, France), *Mar. Chem.*, *95*, 271–281.

Fennel, K., M. Follows, and P. G. Falkowski (2005), The co-evolution of the nitrogen, carbon and oxygen cycles in the Proterozoic ocean, *Am. J. Sci.*, *305*(6–8), 526–545.

Galli, M. T., F. Jadoul, S. M. Bernasconi, and H. Weissert (2005), Anomalies in global carbon cycling and extinction at the Triassic/Jurassic boundary: Evidence from a marine C-isotope record, *Palaeogeogr. Palaeoclimatol. Palaeoecol.*, *216*, 203–214.

Galli, M. T., F. Jadoul, S. M. Bernasconi, S. Cirilli, and H. Weissert (2007), Stratigraphy and palaeoenvironmental analysis of the Triassic–Jurassic transition in the western Southern Alps (Northern Italy), *Palaeogeogr. Palaeoclimatol. Palaeoecol.*, *244*(4–9), 52–70.

Ganeshram, R. S., T. F. Pedersen, S. E. Calvert, and J. W. Murray (1995), Large changes in oceanic nutrient inventories from glacial to interglacial periods, *Nature*, *376*, 755–758.

Ganeshram, R. S., T. F. Pedersen, S. E. Calvert, G. W. McNeill, and M. R. Fontugne (2000), Glacial-interglacial variability in denitrification in the world's oceans: Causes and consequences, *Paleoceanography*, *15*(4), 361–376.

Ganeshram, R. S., T. F. Pedersen, S. E. Calvert, and R. François (2002), Reduced nitrogen fixation in the glacial ocean inferred from changes in marine nitrogen and phosphorus inventories, *Nature*, *415*, 156–159.

Gomez, J. J., A. Goy, and E. Barron (2007), Events around the Triassic-Jurassic boundary in northern and eastern Spain: A review, *Palaeogeogr. Palaeoclimatol. Palaeoecol.*, *244*(1–4), 89–110.

Guex, J., A. Bartolini, V. Atudorei, and D. Taylor (2004), High-resolution ammonite and carbon isotope stratigraphy across the Triassic-Jurassic boundary at New York Canyon (Nevada), *Earth Planet. Sci. Lett.*, *225*, 29–41.

Hallam, A. (2001), A review of the broad patter of Jurassic sea-level changes and their possible causes in the light of current knowledge, *Palaeogeogr. Palaeoclimatol. Palaeoecol.*, *167*, 23–37.

Hallam, A. (2002), How catastrophic was the end-Triassic mass extinction?, *Lethaia*, *35*, 147–157.

Hallam, A., and P. B. Wignall (1999), Mass extinctions and sea-level changes, *Earth Sci. Rev.*, *48*(4), 217–250.

Hallam, A., and P. B. Wignall (2000), Facies changes across the Triassic-Jurassic boundary in Nevada, USA, *J. Geol. Soc. London*, *157*, 49–54.

Hesselbo, S. P., S. A. Robinson, F. Surlyk, and S. Piasecki (2002), Terrestrial and marine extinction at the Triassic-Jurassic boundary synchronized with major carbon-cycle perturbation: A link to initiation of massive volcanism?, *Geology*, *30*, 251–254.

Hesselbo, S. P., C. A. McRoberts, and J. Pálfy (2007), Triassic-Jurassic boundary events: Problems, progress, possibilities, *Palaeogeogr. Palaeoclimatol. Palaeoecol.*, *244*, 1–10.

Hettich, M. (1974), Ein Vollständiges Rhät/Lias-Profil aus der Langenbrückener Senke, Baden-Württemberg (Kernbohrung Mongolsheim 1968), *Geol. Jahrbuch*, *A16*, 75–105.

Huynh, T. T., and C. J. Poulsen (2005), Rising atmospheric CO_2 as a possible trigger for the end-Triassic mass extinction, *Palaeogeogr. Palaeoclimatol. Palaeoecol.*, *217*, 223–242.

Jenkyns, H. C., D. R. Gröcke, and S. P. Hesselbo (2001), Nitrogen isotopic evidence for water mass denitrification during the early Toarcian (Jurassic) oceanic anoxic event, *Paleoceanography*, *16*(6), 593–603.

Kidder, D. L., and T. R. Worsley (2004), Causes and consequences of extreme Permo-Triassic warming to globally equable climate and relation to the Permo-Triassic extinction and recovery, *Palaeogeogr. Palaeoclimatol. Palaeoecol.*, *203*, 207–237.

Kiessling, W., M. Aberhan, B. Brenneis, and P. J. Wagner (2007), Extinction trajectories of benthic organisms across the Triassic-Jurassic boundary, *Palaeogeogr. Palaeoclimatol. Palaeoecol.*, *244*(1–4), 201–222.

Knight, K. B., S. Nomade, P. R. Renne, A. Marzoli, H. Bertrand, and N. Youbi (2004), The Central Atlantic magmatic province at the Triassic-Jurassic boundary: Paleomagnetic and $^{40}Ar/^{39}Ar$ evidence from Morocco for brief, episodic volcanism, *Earth Planet. Sci. Lett.*, *228*, 143–160.

Kuerschner, W. M., N. R. Bonis, and L. Krystyn (2007), Carbon-isotope stratigraphy and palynostratigraphy of the Triassic-Jurassic transition in the Tiefengraben section - Northern Calcareous Alps (Austria), *Palaeogeogr. Palaeoclimatol. Palaeoecol.*, *244*, 257–280.

Marzoli, A., et al. (2004), Synchrony of the Central Atlantic magmatic province and the Triassic-Jurassic boundary climatic and biotic crisis, *Geology*, *32*(11), 973–976.

McElwain, J. C., D. J. Beerling, and F. I. Woodward (1999), Fossil plants and global warming at the Triassic-Jurassic boundary, *Science*, *285*, 1386–1390.

McHone, J. G. (2002), Volatile emissions of Central Atlantic magmatic province basalts: Mass assumptions and environmental consequences, in *The Central Atlantic Magmatic Province*, edited by W. E. Hames et al., pp. 241–254, American Geophysical Union, Geophysical Monograph.

McRoberts, C. A., H. Furrer, and D. S. Jones (1997), Palaeoenvironmental interpretation of a Triassic-Jurassic boundary section from Western Austria based on palaeoecological and geochemical data, *Palaeogeogr. Palaeoclimatol. Palaeoecol.*, *136*, 79–95.

Mills, K. H., and D. W. Schindler (1986), Biological indicators of lake acidification, *Water Air Soil Pollut.*, *30*, 779–789.

Morford, J. L., and S. Emerson (1999), The geochemistry of redox sensitive trace metals in sediments, *Geochim. Cosmochim. Acta*, *63*(11/12), 1735–1750.

Olsen, P. E., D. V. Kent, H.-D. Sues, C. Koebert, H. Huber, A. Montanari, E. C. Rainforth, S. J. Fowell, M. J. Szajna, and B. W. Hartline (2002), Ascent of dinosaurs linked to an iridium anomaly at the Triassic-Jurassic boundary, *Science*, *296*, 1305–1307.

Pálfy, J. (2003), Volcanism of the Central Atlantic magmatic province as a potential driving force in the end-Triassic mass extinction, *Geophys. Monogr.*, *136*, 255–267.

Pálfy, J., A. Demény, J. Haas, M. Hetényi, M. J. Orchard, and I. Vető (2001), Carbon isotope anomaly and other geochemical changes at the Triassic-Jurassic boundary from a marine section in Hungary, *Geology*, *29*, 1047–1050.

Pálfy, J., et al. (2007), Triassic-Jurassic boundary events inferred from integrated stratigraphy of the Csővár section, Hungary, *Palaeogeogr. Palaeoclimatol. Palaeoecol.*, *244*, 11–33.

Plank, T., and C. H. Langmuir (1998), The chemical composition of subducting sediment and its consequences for the crust and mantle, *Chem. Geol.*, *145*, 325–394.

Raiswell, R., R. Newton, and P. B. Wignall (2001), An indicator of water-column anoxia: Resolution of biofaces variations in the Kimmeridge Clay (Upper Jurassic, U. K.), *J. Sediment. Res.*, *71*(2), 286–294.

Robock, A. (2000), Volcanic eruptions and climate, *Rev. Geophys.*, *38*(2), 191–219.

Sephton, M. A., K. Amor, I. A. Franchi, P. B. Wignall, R. Newton, and J.-P. Zonneveld (2002), Carbon and nitrogen isotope disturbances and an end-Norian (Late Triassic) extinction event, *Geology*, *30*(12), 1119–1122.

Stokes, P. M. (1986), Ecological effects of acidification on primary producers in aquatic systems, *Water Air Soil Pollut.*, *30*, 421–438.

Tanner, L. H., S. G. Lucas, and M. G. Chapman (2004), Assessing the record and causes of Late Triassic extinctions, *Earth Sci. Rev.*, *65*, 103–139.

Taylor, S. R., and S. M. McLennan (1985), *The Continental Crust: Its Composition and Evolution*, 312 pp., Blackwell Scientific Publications, Oxford.

Tribovillard, N., T. J. Algeo, T. W. Lyons, and A. Riboulleau (2006), Trace metal as paleoredox and paleoproductivity proxies: An update, *Chem. Geol.*, *232*, 12–32.

Twitchett, R. J. (2006), The palaeoclimatology, palaeoecology, and palaeoenvironmental analysis of mass extinction events, *Palaeogeogr. Palaeoclimatol. Palaeoecol.*, *232*, 190–213.

van de Schootbrugge, B., F. Tremolada, Y. Rosenthal, T. R. Bailey, S. Feist-Burkhardt, H. Brinkhuis, J. Pross, D. V. Kent, and P. G. Falkowski (2007), End-Triassic calcification crisis and blooms of organic-walled "disaster species", *Palaeogeogr. Palaeoclimatol. Palaeoecol.*, *244*(1–4), 126–141.

Vaughan, A. P. M., and B. C. Storey (2007), A new supercontinent self-destruct mechanism: Evidence from the late Triassic-early Jurassic, *J. Geol. Soc.*, *164*, 383–392.

von Hildebrandt, L., and V. Schweizer (1992), Zur biostratigraphischen Gliederung des Unteren Jura in der Langenbrückener Senke (Baden-Württemberg, Südwestdeutschland), *Jahresbericht und Mitteilungen der oberrheinischen geologischen Verein, NF*, *74*, 215–236.

Wada, E. (1980), Nitrogen isotope fractionation and its significance in biogeochemical processes occuring in marine environments, in *Isotope Marine Chemistry*, edited by E. D. Goldberg and Y. Horibe, pp. 375–398, Uchida Rokakuho Publ. Co. Ltd., Tokyo.

Ward, P. D., J. W. Haggart, E. S. Carter, D. Wilbur, H. W. Tipper, and T. Evans (2001), Sudden productivity collapse associated with the Triassic-Jurassic boundary mass extinction, *Science*, *292*, 1148–1151.

Ward, P. D., G. H. Garrison, J. W. Haggart, D. A. Kring, and M. J. Beattie (2004), Isotopic evidence bearing on Late Triassic extinction events, Queen Charlotte Islands, British Columbia, and implications for the duration and cause of the Triassic/Jurassic mass extinction, *Earth Planet. Sci. Lett.*, *224*, 589–600.

Whiteside, J. H., P. E. Olsen, D. V. Kent, S. J. Fowell, and M. Et-Touhami (2007), Synchrony between the Central Atlantic magmatic province and the Triassic-Jurassic mass-extinction event?, *Palaeogeogr. Palaeoclimatol. Palaeoecol.*, *244*(1–4), 345–367.

Williford, K. H., P. D. Ward, G. H. Garrison, and R. Buick (2007), An extended organic carbon-isotope record across the Triassic-Jurassic boundary in the Queen Charlotte Islands, British Columbia, Canada, *Palaeogeogr. Palaeoclimatol. Palaeoecol.*, *244*, 290–296.

P. G. Falkowski, M. P. Field, T. M. Quan, and Y. Rosenthal, Institute of Marine and Coastal Sciences, Rutgers University, 71 Dudley Road, New Brunswick, NJ 08901, USA. (quan@marine.rutgers.edu)

B. van de Schootbrugge, Institute of Geosciences, Johann Wolfgang Goethe University Frankfurt, Altenhöfer Allee 1, D-60438 Frankfurt, Germany.